Mineralogical Magazine, August 2013, Vol. 77(6), pp. 2773–2792

Oxo-magnesio-hastingsite, $NaCa_2(Mg_2Fe_3^{3+})(Al_2Si_6)O_{22}O_2$, a new anhydrous amphibole from the Deeti volcanic cone, Gregory rift, northern Tanzania

A. N. Zaitsev[1,2,*], E. Yu. Avdontseva[3], S. N. Britvin[3], A. Demény[4], Z. Homonnay[5], T. E. Jeffries[2], J. Keller[6], V. G. Krivovichev[1], G. Markl[7], N. V. Platonova[3], O. I. Siidra[3], J. Spratt[2] and T. Vennemann[8]

[1] Department of Mineralogy, Faculty of Geology, St. Petersburg State University, University Emb. 7/9, St. Petersburg, 199034 Russia
[2] Imaging and Analysis Centre, Department of Earth Sciences, Natural History Museum, Cromwell Road, London SW7 5BD, UK
[3] Department of Crystallography, Faculty of Geology, St. Petersburg State University, University Emb. 7/9, St. Petersburg, 199034 Russia
[4] Institute for Geological and Geochemical Research, Research Centre for Astronomy and Earth Sciences, Hungarian Academy of Sciences, Budaörsi út 45., H-1112, Budapest, Hungary
[5] Institute of Chemistry, Faculty of Science, Eötvös Loránd University, Pázmány P. s. 1/A, 1117 Budapest, Hungary
[6] Institut für Geowissenschaften Mineralogie-Geochemie, Universität Freiburg, Albertstrasse 23b, D-79104 Freiburg, Germany
[7] Fachbereich Geowissenschaften, Universität Tübingen, Wilhelmstrasse 56, D-72074 Tübingen, Germany
[8] Institute of Mineralogy and Geochemistry, University of Lausanne, Anthropole, CH-1015, Lausanne, Switzerland

[*Received 17 January 2013; Accepted 22 June 2013; Associate Editor: F. Hawthorne*]

ABSTRACT

Oxo-magnesio-hastingsite, ideally $NaCa_2(Mg_2Fe_3^{3+})(Al_2Si_6)O_{22}O_2$, is a new anhydrous amphibole from the Deeti volcanic cone in the Gregory rift (northern Tanzania). The mineral occurs as megacrysts up to 12 cm in size in crystal-rich tuff. Oxo-magnesio-hastingsite is brown with a vitreous lustre and has a perfect {110} cleavage. The measured density is 3.19(1) g/cm^3. Ferri-kaersutite is biaxial (−), $\alpha = 1.706$ (2), $\beta = 1.715(2)$, $\gamma = 1.720(2)$ (Na light, 589 nm). 2V (calc.) = 73º. Dispersion: r > v, weak; orientation: Y = *b*; Z^*c* = 8º; pleochroism: strong, Z: dark brown, Y: brown, X: light brown. The average chemical formula of the mineral derived from electron microprobe analyses, Mössbauer spectroscopy and direct water determination is $(Na_{0.67}K_{0.33})_{\Sigma 1.00}(Ca_{1.87}Na_{0.14}Mn_{0.01})_{\Sigma 2.02}(Mg_{3.27}Fe^{3+}_{1.25}Ti_{0.44}Al_{0.08})_{\Sigma 5.04}(Al_{1.80}Si_{6.20}O_{22})(O_{1.40}OH_{0.60})_{\Sigma 2.00}$. It has monoclinic symmetry, space group *C*2/*m* and unit-cell parameters $a = 9.8837(3)$, $b = 18.0662(6)$, $c = 5.3107(2)$ Å, $\beta = 105.278(1)^o$, $V = 914.77(5)$ Å^3, $Z = 2$. The five strongest powder-diffraction lines [*d* in Å , (*I*/*I*o), *hkl*] are: 3.383 (62) (131), 2.708 (97) (151), 2.555 (100) ($\bar{2}02$), 2.349 (29) ($\bar{3}51$) and 2.162 (36) (261). The isotopic composition of H and O, as well as the concentration of trace elements in oxo-magnesio-hastingsite suggest its formation from a melt originated from a mantle source metasomatized by slab-derived fluids.

Keywords: oxo-magnesio-hastingsite, oxo amphibole group, new mineral, Mössbauer and IR spectroscopy, chemical composition, X-ray diffraction, crystal structure, H and O isotopic composition, Deeti cone, Gregory rift, Tanzania.

Introduction

The Lake Natron–Engaruka area in the Gregory rift, northern Tanzania, is a well known volcanic

* E-mail: burbankite@gmail.com
DOI: 10.1180/minmag.2013.077.6.06

field, primarily due to the activity of Oldoinyo Lengai volcano that has historically erupted carbonatitic and nephelinitic rocks (e.g. Wakefield, 1870; Dawson, 1962, 2008; Keller and Krafft, 1990; Bell and Keller, 1995; Keller *et al.*, 2010; Keller and Zaitsev, 2012). Kerimasi is another large, but extinct, carbonatitic volcano in this area (Dawson, 1964; Mariano and Roeder, 1983; Hay, 1983; Church, 1996; Reguir *et al.*, 2008; Zaitsev, 2010) together with a further 200 smaller volcanic cones, explosion craters and lava flows (Dawson and Powell, 1969; Hay, 1983; Dawson and Smith, 1988; Johnson *et al.*, 1997; Keller *et al.*, 2006; Zaitsev *et al.*, 2010, 2011; Mattsson and Tripoli, 2011).

Silicate effusive rocks occurring at these volcanic complexes are both primitive and evolved varieties including olivine melilitites, olivine-melilite nephelinites, melilite nephelinites, combeite-wollastonite nephelinites, nephelinites, phonolitic nephelinites and phonolites (Dawson *et al.*, 1985; Keller *et al.*, 2006). Pyroclastic rocks, which are more abundant than lavas, are represented by ashes, tuffs (massive, lapilli, lithic and crystal-rich varieties) and agglomerates (Dawson and Powell, 1969; Hay, 1983; Mattsson and Tripoli, 2011). Crystal-rich tuff (olivine ± clinopyroxene ± amphibole ± mica ± melilite) is a common rock type in several small cones and craters including Loolmurwak, Kisete, Loluni and Deeti (Fig. 1). The last named contains unusually large amphibole megacrysts, described as pargasite and hornblende-pargasite by Johnson *et al.* (1997). A detailed mineralogical, spectroscopic and crystal-chemical study of this mineral provided evidence that it is a new mineral of the amphibole supergroup, and in particular of the oxo-amphibole group.

The new mineral and the mineral name have been approved by the Commission on New Minerals and Mineral Names of the IMA, proposal 2011-035 (Williams *et al.*, 2011). In reference to the new IMA report on amphibole nomenclature (Hawthorne *et al.*, 2012), the mineral was renamed (from ferrikaersutite to oxo-magnesio-hastingsite). The formula was also modified (from $NaCa_2(Mg_3Fe^{3+}Ti)(Al_2Si_6)O_{22}O_2$ to $NaCa_2(Mg_2Fe_3^{3+})(Al_2Si_6)O_{22}O_2$) by the IMA-CNMNC Subcommittee on amphiboles, as ^{C}Ti is < 0.5 a.p.f.u., $^{W}O_{2-}$ is > 1.0 a.p.f.u., Fe^{3+} is dominant over trivalent cations at site *C*, and Mg is dominant over divalent cations also at site *C*. The cotype specimen is deposited in the Mineralogical Museum, Department of Mineralogy, St. Petersburg State University, St. Petersburg, Russia (sample OL 22, catalogue number 1/19465).

Amphibole occurrence, morphology and properties

The samples studied of oxo-magnesio-hastingsite (OL 22 and OL 22 AZ) were collected from the lower slope on the southeastern part of the tuff ring of the highly eroded Deeti volcanic cone (Fig. 2). The host rocks are melilititic massive tuffs that contain a suite of cm-size megacrysts (diopside and phlogopite in addition to amphibole) and xenoliths of amphibole-mica peridotites, pyroxenites and ijolites (Johnson *et al.*, 1997). Additional samples of amphibole are from lapilli tuff of the Deeti cone (southwestern part of the tuff ring, sample DT -/11, Fig. 2) and crystal-rich tuffs of the Loolmurwak (sample OL 313) and Loluni (samples LL 1/5, -/4 and 3/4) craters. Two amphibole samples were collected from the lower northern and eastern slopes of the Oldoinyo Lengai volcano – the Dorobo canyon (sample OL 246) and a gully between Eastern Chasm and the Lalarasi cone (sample OL 165) (Fig. 1). Both samples are from black melilite-bearing crystal-rich tuffs which are known as Unit II "Biotite-Pyroxene-Tuffs" (Dawson, 1962) and "Olivine-Biotite-Pyroxene Tuffs" (Wiedenmann *et al.*, 2010).

Oxo-magnesio-hastingsite occurs as megacrysts up to 12 cm in size (Fig. 3). All samples are single crystals, rounded, do not show any crystal faces, and they are characterized by a smooth (''melted'') surface. Rarely, oxo-magnesio-hastingsite crystals contain inclusions of euhedral diopside grains. The amphibole is brown with a white streak; small fragments are transparent and have a vitreous lustre. Oxo-magnesio-hastingsite is brittle, has a perfect {110} cleavage and uneven fracture. The Mohs hardness is ~6. The measured mineral density (hydrostatic weighing) is 3.19(2) g/cm^3 while the calculated density from the average chemical and X-ray data is 3.219 g/cm^3.

Oxo-magnesio-hastingsite is biaxial (–), α = 1.706 (2), β = 1.715(2), γ = 1.720 (2) (Na light, 589 nm). 2V (calc.) = 73º. Dispersion: r > v, weak; orientation: Y = *b*; Z ^ *c* = 8º; pleochroism: strong, Z: dark brown, Y: brown, X: light brown. Compatibility index, $1 - (K_p/K_c)$, is equal to −0.002 (superior).

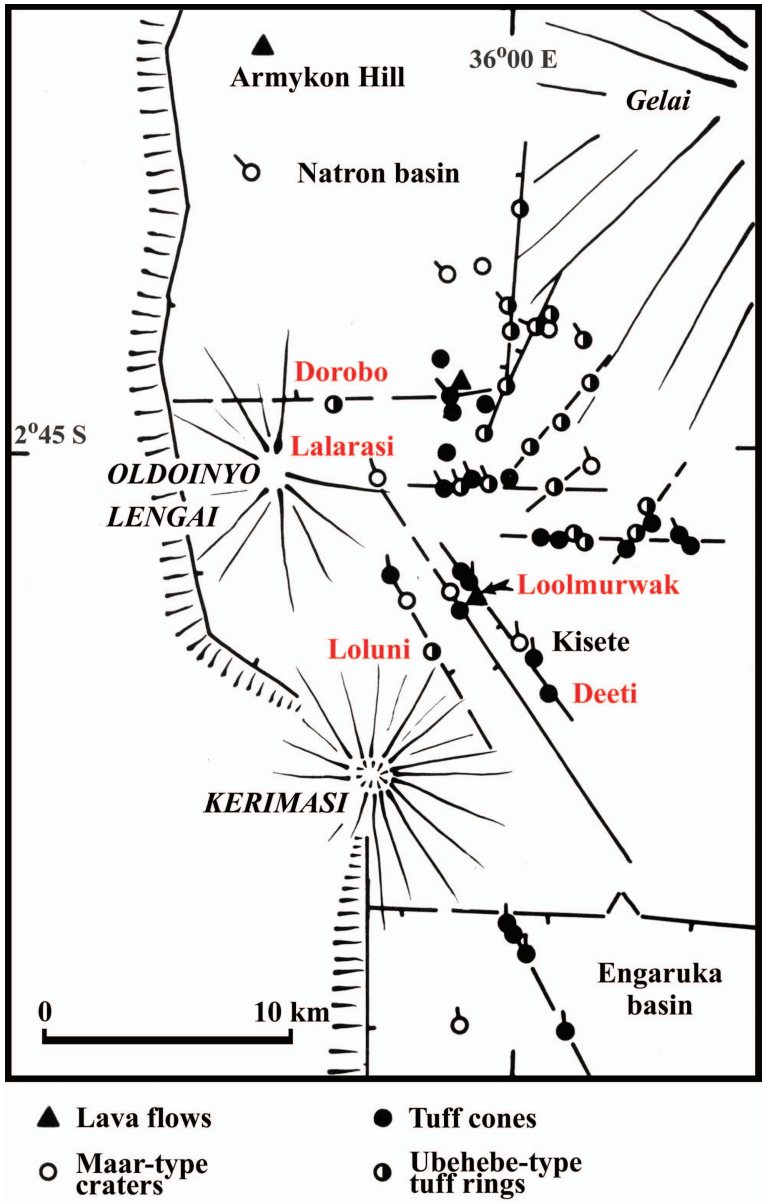

FIG. 1. Location of volcanoes, volcanic cones and explosive craters in the Lake Natron–Engaruka area (after Dawson and Powell (1969)); a more detailed map is given by Mattsson and Tripoli (2011).

Mössbauer and IR spectroscopy

The Mössbauer spectra of the oxo-magnesio-hastingsite (OL 22) and amphibole samples from Loolmurwak (OL 313) and Oldoinyo Lengai-Dorobo (OL 246) (Fig. 4) were recorded at room temperature in constant acceleration mode with a Wissel spectrometer using a ^{57}Co(Rh) source at the Laboratory of Nuclear Chemistry, Eötvös Lorand University, Budapest. The samples were powdered carefully in order to avoid non-random orientation of crystallites that would result in asymmetrical doublets in the Mössbauer spectra. To eliminate any residual texture the disc-shaped thin samples were mounted in the 'magic angle'

FIG. 2. Deeti cone (*a*) view towards the northwest; the arrow indicates (*b*) where bedded pyroclasticic rocks are well exposed; photos (*a*) by Anatoly Zaitsev (2000) and (*b*) by Barry Dawson (2007).

FIG. 3. Oxo-magnesio-hastingsite megacryst (sample OL 22 AZ, crystal size 5−8−10 cm); photo by Polina Zaitseva.

geometry (54.7 degree between the gamma radiation and the normal vector of the plane of the absorber). The spectra could then be safely evaluated by assuming symmetrical doublets by least-squares fitting of Lorentzian lines using the *MössWinn* program. Line widths were constrained to be the same within one evaluation. Isomer shifts are given relative to α-Fe.

For the oxo-magnesio-hastingsite sample, a two doublet evaluation resulted in a satisfactory fit. Both isomer shifts (with reference to α-Fe at room temperature) indicate Fe^{3+} unambiguously. No traces of Fe^{2+} can be observed. The two types of Fe^{3+} contents were calculated from the relative contributions of the doublets (areas) (Fig. 4, Table 1). Doublet 1 may be assigned to the *M*(1) lattice site and Doublet 2 can be assigned to Fe^{3+} at the *M*(2,3) sites (Nasir and Al Rawas, 2006).

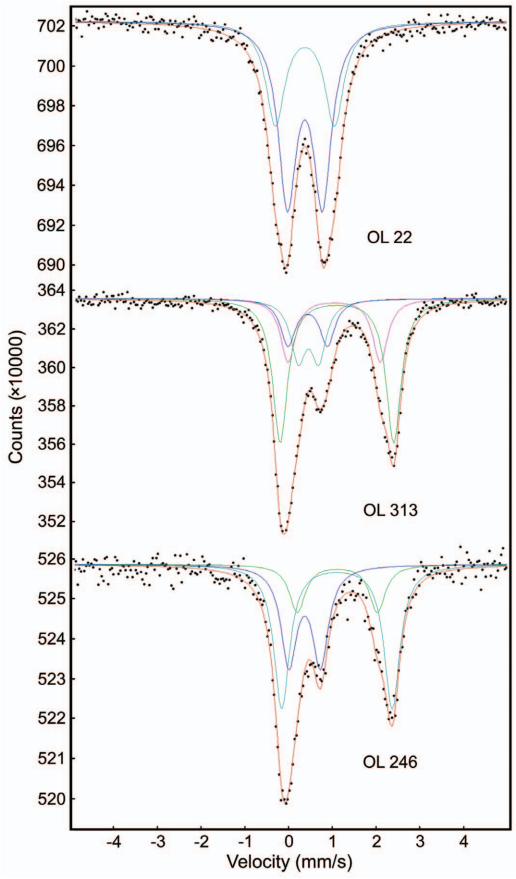

FIG. 4. Mössbauer spectra of oxo-magnesio-hastingsite OL 22 from Deeti, compared to amphibole samples from Loolmurwak (OL 313) and Oldoinyo Lengai (OL 246) recorded at room temperature. The velocity scale refers to α-Fe.

The Mössbauer spectra of the amphiboles from Loolmurwak (sample OL 313) and Oldoinyo Lengai-Dorobo (sample OL 246) (Fig. 4) indicate significant amounts of Fe^{2+} in these samples, 66.6% and 66.3%, respectively (Table 1). These percentage values are based on spectrum areas, disregarding the possible differences in Mössbauer-Lamb factors at the different lattice sites.

The IR spectra of the oxo-magnesio-hastingsite (samples OL 22 and OL 22 AZ) were recorded using a Bruker Vertex 70 FTIR spectrophotometer at the Crystallography Department, St Petersburg State University (KBr pellet, resolution 4 cm^{-1}). The spectra are identical and have sets of bands that are typical for amphiboles in the 300–1400 cm^{-1} region: 460–508–633–664–681–737–940–975–1055 cm^{-1} (Fig. 5) (Apopei *et al.*, 2011 and references herein). Very weak bands were observed in the OH-stretching region between 3000 and 4000 cm^{-1} (Fig. 5) with a maximum around 3662 cm^{-1} and additional bands at 3652 and 3645 cm^{-1}. The oxo-magnesio-hastingsite spectra are similar, but not identical, to those of Ti-rich pargasite with small water contents (Della Ventura *et al.*, 2007). Observed bands for the oxo-magnesio-hastingsite can be correlated with bands D and E in Ti-rich pargasite, which were assigned due to the presence of Fe^{3+} and Ti at *M* sites, and $(OH)^-$ and O^{2-} in a local configuration around the *A* site (Della Ventura *et al.*, 2007)

Chemical composition

Chemical analyses of amphibole from the Deeti, Loolmurwak, Loluni, Dorobo and Lalarasi cones and craters were carried out using a Cameca SX-100 electron microprobe located at the Natural History Museum, London, UK (wave-dispersive mode, 20 kV, 20 nA, 5 μm beam diameter). Probe standards include diopside (Si), $MnTiO_3$ (Ti, Mn), corundum (Al), hematite (Fe), periclase (Mg), wollastonite (Ca), jadeite (Na), KBr (K), chromite (Cr), NiO (Ni), topaz (F), halite (Cl), celestine (S) and $ScPO_4$ (P). Trace elements in amphibole were determined by LA ICP-MS, using an ESI New Wave 193FX laser ablation accessory (lambda = 193 nm, fluence 2.8 J/cm^2, 50 μm beam diameter) coupled to an Agilent 7500cs quadrupole-based mass spectrometer. The National Institute of Standards Technology SRM 612 was used as a calibration standard. CaO determined by electron probe was used as an internal standard. H_2O was determined by vacuum heating in a silica tube followed by conversion to H_2 gas by H_2O-Zn reaction (Vennemann and O'Neil, 1993). The precision of the H_2O content is better than 0.1 wt.%, on the basis of repeated measurements of NBS-30 biotite and in-house standards. Direct determination of FeO content in the ferrikaersutite (sample OL 22 AZ) was made by wet chemistry (titration) at VSEGEI, St Petersburg (total iron was determined by XRF analysis) and water content was determined by the Alimarin method using absorption tubes filled with anhydrous magnesium perchlorate (Institute of Problems of Chemical Physics, Chernogolovka).

TABLE 1. Mössbauer parameters of the amphibole samples.

	Isomer shift (mm/s)	Quadrupole splitting (mm/s)	FWHM (mm/s)	Relative intensity (%)	Fe species
OL 22					
Doublet 1	0.380(3)	0.81(1)	0.51(1)	65(2)	Fe^{3+}
Doublet 2	0.380(5)	1.37(2)	0.51(1)	35(2)	Fe^{3+}
OL 313					
Doublet 1	0.44(3)	0.90(6)	0.410(7)	14.8	Fe^{3+}
Doublet 2	0.460(7)	0.47(2)	0.410(7)	18.6	Fe^{3+}
Doublet 3	1.111(2)	2.594(8)	0.410(7)	46.2	Fe^{2+}
Doublet 4	1.05(2)	2.11(4)	0.410(7)	20.4	Fe^{2+}
OL 246					
Doublet 1	0.37(1)	0.72(2)	0.43(1)	33.7	Fe^{3+}
Doublet 2	1.111(6)	2.52(2)	0.43(1)	49.8	Fe^{2+}
Doublet 3	1.12(2)	1.83(5)	0.43(1)	16.5	Fe^{2+}

Average chemical compositions of the amphiboles studied are given in Table 2 (major and minor elements) and Table 3 (trace elements). Crystal-chemical formulae were calculated on the basis of 24(O,OH) only for samples where Fe^{3+}/Fe^{2+} ratios were determined by Mössbauer spectroscopy. According to the calculated empirical mineral formulae (Table 2) and new amphibole classification (see Introduction) oxo-magnesio-hastingsite from Deeti has an ideal endmember formula $NaCa_2(Mg_2Fe^{3+}_3)(Al_2Si_6)O_{22}O_2$ while amphibole from Loolmurwak and Dorobo is Ti-rich magnesio-hastingsite.

A correct formula calculation for other samples is impossible due to unknown Fe^{3+}/Fe^{2+} ratios and the small water content (the latter implies the presence of significant O^{2-} in the *W* site which results in incorrect formula calculations on the basis of charge balance). Similarity in the contents of major and minor elements suggests that the mineral is also magnesio-hastingsite or kaersutite (particularly samples from Loluni with a large Ti content).

A characteristic feature of the oxo-magnesio-hastingsite from the Deeti cone is its small water content – 0.61 wt.% (sample OL 22) and 0.405 wt.% (sample OL 22 AZ). Magnesio-

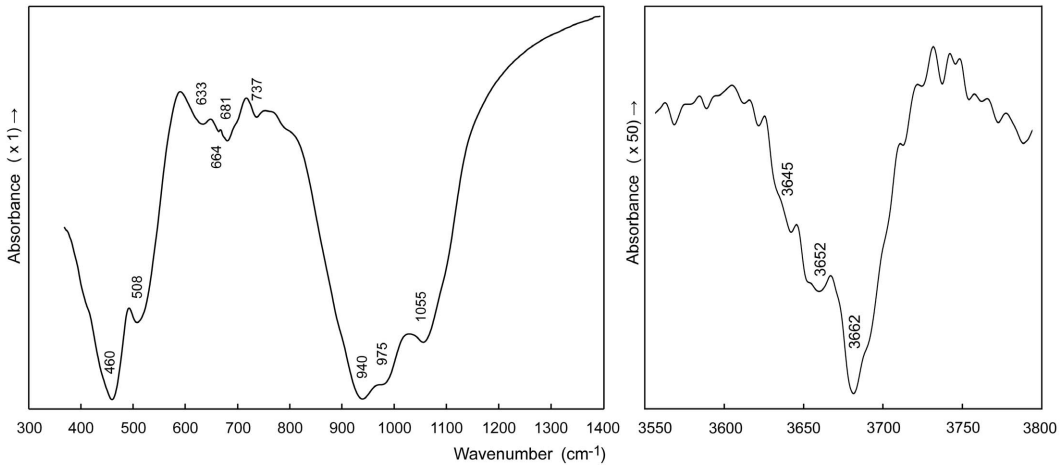

FIG. 5. Infrared spectrum of the oxo-magnesio-hastingsite (sample OL 22).

TABLE 2. Average major and minor element compositions for oxo-magnesio-hastingsite and magnesio-hastingsite.

Sample	OL 22	DT -/11	OL 313	LL 1/5	LL -/4	LL 3/4	OL 246	OL 165
Locality	Deeti		Loolmurwak	Loluni			Oldoinyo Dorobo	Lengai Lalarasi
N	17	14	7	8	6	9	9	11
Oxide (wt.%)								
SiO_2	41.89	42.16	42.06	40.93	40.80	41.06	40.29	38.89
TiO_2	3.96	3.94	3.92	4.48	4.63	4.59	4.34	3.57
Al_2O_3	10.75	10.75	10.99	11.61	11.46	11.50	11.88	13.45
Fe_2O_3*	11.25		3.39				4.86	
FeO*			6.09				7.84	
FeO**		9.33		10.35	10.22	10.11		11.28
MnO	0.08	0.09	0.09	0.09	0.09	0.08	0.12	0.14
MgO	14.79	15.74	15.06	14.52	14.51	14.81	13.09	13.75
CaO	11.76	11.85	11.79	11.88	11.85	11.92	11.80	12.32
Na_2O	2.84	2.83	2.71	2.60	2.66	2.66	2.76	2.64
K_2O	1.74	1.72	1.74	1.94	1.91	1.82	1.66	1.74
H_2O	0.61	1.03	1.40	1.48	1.48	1.47	1.30	1.51
Total	99.67	99.44	99.24	99.88	99.60	100.03	99.94	99.32
a.p.f.u.								
Si	6.20		6.23				6.03	
Al	1.80		1.77				1.97	
Total	8.00		8.00				8.00	
Mg	3.27		3.33				2.92	
Fe^{3+}	1.25		0.38				0.55	
Fe^{2+}			0.75				0.98	
Ti	0.44		0.44				0.49	
Al	0.08		0.15				0.12	
Total	5.04		5.05				5.06	
Ca	1.87		1.87				1.89	
Na	0.14		0.11				0.12	
Mn	0.01		0.01				0.02	
Total	2.02		1.99				2.03	
Na	0.67		0.67				0.68	
K	0.33		0.33				0.32	
Total	1.00		1.00				1.00	
OH	0.60		1.38				1.30	
O	1.40		0.62				0.70	
Total	2.00		2.00				2.00	

N – number of analyses; * – Fe_2O_3 and FeO calculated from Mössbauer spectra, ** – total Fe as FeO from electron microprobe analyses.

hastingsite and kaersutite from other localities (including another outcrop at the Deeti cone) contains between 1.0 and 1.5 wt.% water (Table 2). Oxo-magnesio-hastingsite is an amphibole with a dominance of Fe^{3+} over Fe^{2+}. The sample OL 22 contains Fe_2O_3 only and the sample OL 22 AZ contains 2.86 wt.% FeO and 8.32 wt.% Fe_2O_3 (Fe^{3+}/Fe_{total} atomic ratio is 0.72); whereas, magnesio-hastingsite from Loolmurwak and Dorobo contains a higher Fe^{2+}/Fe^{3+} ratio, with Fe^{3+} = 0.75–0.98 and Fe^{2+} = 0.38–0.55 a.p.f.u. (Table 2). All amphiboles are titanium-rich and only a small amount of octahedral aluminium is present.

TABLE 3. Average trace element compositions for oxo-magnesio-hastingsite and magnesio-hastingsite.

Sample	OL 22	DT -/11	OL 313	LL 1/5	LL -/4	LL 3/4	OL 246	OL 165
Locality	Deeti		Loolmurwak	Loluni			Oldoinyo Dorobo	Lengai Lalarasi
N	4	4	4	4	4	4	4	4
Element (ppm)								
Mn	695	663	600	717	709	704	821	1063
Sr	357	391	331	508	416	372	442	616
V	253	249	272	294	321	312	316	153
Ba	194	191	162	293	267	243	292	503
Zr	128	121	116	115	82.6	73.1	153	795
Sc	82.0	92.7	79.0	63.0	62.4	61.0	44.9	31.0
Ni	74.2	93.5	168	116	111	115	64.9	13.9
Cr	41.7	59.4	237	171	43.4	47.6	96.7	21.3
Co	55.7	58.6	53.8	65.0	63.2	62.9	56.5	42.6
Zn	54.4	61.3	51.0	62.4	59.2	59.0	63.1	68.2
Li	38.8	<7.37	<14.6	<8.96	<9.53	<12.2	<15.7	<12.9
Nb	21.1	21.0	19.3	21.9	18.3	17.1	25.2	46.9
Y	7.39	6.86	7.70	8.00	6.81	6.26	9.12	16.0
Cu	5.41	6.64	5.83	6.06	6.10	6.21	4.48	4.24
Rb	6.54	7.26	7.20	10.2	9.87	9.38	6.41	7.29
Hf	5.94	5.47	5.48	5.21	4.05	3.33	6.44	19.8
Ta	1.94	1.90	1.66	1.83	1.69	1.57	2.22	2.07
Mo	0.28	0.35	0.27	0.34	0.35	0.33	0.36	0.47
Pb	0.21	0.24	0.20	0.27	0.25	0.24	0.25	0.29
Th	0.05	0.08	0.05	0.06	0.05	0.05	0.05	0.04
La	7.53	6.73	7.17	8.51	6.66	5.63	8.21	14.6
Ce	22.0	20.4	22.7	25.6	18.4	17.3	23.6	36.9
Pr	3.72	3.38	3.87	4.08	2.91	2.69	4.09	5.80
Nd	18.6	16.5	19.2	19.3	13.9	12.7	20.5	27.2
Sm	4.25	3.81	4.65	4.36	3.14	2.91	4.87	7.05
Eu	1.30	1.19	1.40	1.40	0.99	0.98	1.50	2.36
Gd	3.44	3.08	3.66	3.44	2.59	2.35	4.02	6.49
Tb	0.41	0.39	0.44	0.44	0.33	0.30	0.49	0.81
Dy	2.11	1.93	2.19	2.18	1.79	1.57	2.54	4.21
Ho	0.33	0.31	0.33	0.34	0.30	0.26	0.40	0.67
Er	0.68	0.61	0.66	0.73	0.66	0.58	0.80	1.44
Tm	0.08	0.07	0.07	0.09	0.08	0.07	0.10	0.18
Yb	0.45	0.41	0.36	0.52	0.47	0.42	0.58	1.06
Lu	0.06	0.06	0.05	0.07	0.07	0.06	0.08	0.18

N – number of analyses; elements listed in order of their abundances.

On a triangular plot for cations at the *B* site, (Mg-Fe^{3+}-Ti) data points for oxo-magnesio-hastingsite plot near a composition of $Mg_3Fe^{3+}Ti$ and are separated from the composition for that of $Mg_2Fe_3^{3+}$ (Supplementary data, available at www.minersoc.org/pages/e_journals/dep_mat_mm.html). This indicates the presence of a significant amount of the ferri-kaersutite $NaCa_2(Mg_3Fe^{3+}Ti)(Al_2Si_6)O_{22}O_2$ endmember, which predominates over the oxo-magnesio-hastingsite $(Na,K)Ca_2(Mg_2Fe_3^{3+})(Al_2Si_6)O_{22}O_2$ endmember – 44 *vs.* 26 mol.%, respectively. The remaining 30 mol.% of endmembers are potassium analogues of ferri-katophorite (3 mol.%), katophorite (8 mol.%), edenite (17 mol.%), and 2 mol.% are unassigned. The endmember compositions are, however, quite different for the calculation having oxo-magnesio-hastingsite as major component (42 mol.%), the other endmembers are hypothe-

tical Ti-bearing components $(Na,K)Ca_2(Mg_4Ti)(AlSi_7O_{22})O_2$ (28 mol.%), $K(NaCa)_2(Mg_4Ti)(Al_2Si_6O_{22})(OH)_2$ (14 mol.%), potassium analogue of edenite (15 mol.%), and 2 mol.% are unassigned (Supplementary data).

Similar sodium-calcium-magnesium amphiboles with large Fe^{3+} and Ti^{4+}, and small water contents are known from several localities (e.g. Dawson and Smith, 1982). They have been described as "titaniferous pargasite and kaersutite" (Dawson and Smith, 1982), "oxykaersutite" (Dyar *et al.*, 1993) or "ferrikaersutite" (Nasir and Al-Rawas, 2006).

Oxo-magnesio-hastingsite and other amphiboles contain various trace elements, and the minerals from Deeti, Loolmurwak, Loluni and Oldoinyo Lengai-Dorobo show comparable variations in element contents and nearly identical element ratios (e.g. Nb/Ta, Zr/Hf); whereas the mineral from Oldoinyo Lengai-Lalarasi is characterized by relative enrichment or depletion in element contents, and accordingly higher or lower element ratios (Table 3). The minerals are relatively enriched in Mn, Sr, V, Ba, Zr, Sc, Ni, Cr and *REE* ($\leqslant$1063 ppm), depleted in Co, Zn and Nb ($\leqslant$68 ppm) and contains traces of Y, Cu, Rb, Hf, Ta, Mo, Pb and Th ($\leqslant$20 ppm). Li is present at a detectable level in the oxo-magnesio-hastingsite only (Table 3).

Crystallography

Single-crystal analysis of the oxo-magnesio-hastingsite (0.25 mm × 0.20 mm × 0.20 mm crystal) was performed using a Bruker SMART APEX II diffractometer operated at 50 kV and 40 mA (St Petersburg State University). More than a hemisphere of X-ray diffraction data were collected with frame widths of 0.3º in ω, and with 20 s spent counting for each frame. The data were integrated and corrected for absorption using an empirical ellipsoidal model using the *APEX* and *XPREP* Bruker programs. The unit-cell parameters were refined using least-squares techniques. The atomic coordinates published by Hawthorne and Grundy (1973) were used initially and successfully refined on the basis of F^2 for all unique data in *C*2/*m* space group (monoclinic symmetry) – a = 9.8837(3), b = 18.0662(6), c = 5.3107(2) Å, β = 105.278(1)º, V = 914.77(5) Å^3 and Z = 2. The structure of oxo-magnesio-hastingsite was refined to R_1 = 0.032 for 1907 unique observed reflections with $F^2 \geqslant 4\sigma(F^2)$. The final atom coordinates and anisotropic-displacement parameters are given in Tables 4 and 5, and the list of calculated and observed structure factor data have been deposited with the Principal Editor at http://www.minersoc.org/pages/e_journals/dep_mat_mm.html.

Since the X-ray scattering power of Mg and Al atoms cannot be distinguished, Mg and Al were regarded as one group with one scattering factor. Mg and Al atoms were summed to form Mg* in atomic fractions. For the same reason, Fe^{3+} and Ti were assumed to form a species Fe*. The small amount of Mn was ignored in the process of refinement. Because of the chemical complexity, the following assumptions were employed. Ca was constrained to the *M*(4) site, excess cations (Fe* and Mg*) for the octahedral sites and the rest of the *M*(4) site was filled with Na. The total refined scattering at the *M*(1), *M*(2) and *M*(3) sites is 79.04 electrons per formula unit (e.p.f.u.). The total calculated scattering at these sites is 83.42 e.p.f.u. Thus the refined site occupancies (Table 4) for all *M* sites are in good agreement with chemical data taking into account the close scattering power of located atoms. Generally, bond-distance values (Table 6) obtained for oxo-magnesio-hastingsite are very close to those observed earlier by Hawthorne and Grundy (1973). Note the largest equivalent isotropic-displacement value at the *M*(1) site compare to *M*(2) and *M*(3) sites (Table 4) and the shortest *M*(1)−O distance – *M*(1)−O(3). Both of these observations allow us to consider that all Ti^{4+} is in *M*(1) (Tiepolo *et al.*, 1999), whereas Ti^{4+} is absent in *M*(3). This is also in good agreement with the previous refinements of crystal structures of oxo-amphiboles: ungarettiite (Hawthorne *et al.*, 1995), obertiite (Hawthorne *et al.*, 2000) and dellaventuraite (Tait *et al.*, 2005). The main differences between oxo-magnesio-hastingsite and "oxykaersutite" are observed for the *M*−O(3) bond values which can be explained by the different Al and Fe, OH content in these amphiboles. The *M*−*M* distances with the shortest *M*(1)−*M*(1) bond distance value of 3.0137(10) in oxo-magnesio-hastingsite are in good agreement with the other amphiboles (Hawthorne *et al.*, 1995, 2000; Tait *et al.*, 2005) with large O^{2-} contents instead of OH^- at the O(3) site. The *M*(1)−*M*(2) distance of 3.1493(4)Å in oxo-magnesio-hastingsite also correlates perfectly (Oberti *et al.*, 2007) with the amount of 1.40 a.p.f.u. oxo-component obtained by chemical analyses and IR spectroscopy (see above). The average of *M*(2)−O in oxo-magnesio-hastingsite is less than <*M*(1)−O> and <*M*(3)−O> indicating

TABLE 4. Coordinates and isotropic displacement parameters (Å) of atoms in oxo-magnesio-hastingsite.

Site	Refined site-scattering	Calculated site-scattering	Assigned site-populations	*x*	*y*	*z*	U_{eq}
M(1)	31.7	33.2	$1.22Mg^{2+}+0.44Ti^{4+}+0.34Fe^{3+}$	0	0.08344(3)	½	0.01223(17)
M(2)	31.7	33.6	$1.20Mg^{2+}+0.12Al^{3+}+0.68Fe^{3+}$	0	0.17717(2)	0	0.00715(15)
M(3)	15.4	16.6	$0.67Mg^{2+}+0.33Fe^{3+}$	0	0	0	0.0081(2)
M(4)	37.9	38.7	$1.84Ca^{2+}+0.15Na^{+}+0.01Mn^{2+}$	0.27880(2)	½	0.01131(14)	0.01131(14)
A(m)	6.6	7.4	$Na_{0.67}$	0.0217(7)	½	0.0433(12)	0.0198(12)
A(m')	5.7	6.3	$K_{0.33}$	0.0587(11)	½	0.114(2)	0.0371(17)
T(1)			$Si_{0.575}Al_{0.425}$	0.28190(4)	0.08529(2)	0.30306(7)	0.00740(11)
T(2)			$Si_{0.975}Al_{0.025}$	0.29017(4)	0.17250(2)	0.81059(7)	0.00724(10)
O(1)				0.10780(11)	0.08700(5)	0.21959(19)	0.00988(18)
O(2)				0.11857(11)	0.17148(5)	0.72761(18)	0.00989(18)
O(3)				0.10719(15)	0	0.7145(3)	0.0122(3)
O(4)				0.36486(11)	0.25034(6)	0.7899(2)	0.01222(19)
O(5)				0.34981(11)	0.13882(6)	0.10795(18)	0.0140(2)
O(6)				0.34649(11)	0.11779(6)	0.60676(19)	0.0137(2)
O(7)				0.34140(16)	0	0.2852(3)	0.0172(3)

TABLE 5. Anisotropic displacement parameters (Å) of atoms in oxo-magnesio-hastingsite.

Atom	U_{11}	U_{22}	U_{33}	U_{23}	U_{13}	U_{12}
M(1)	0.0086(3)	0.0209(3)	0.0077(2)	0	0.00317(17)	0
M(2)	0.0073(2)	0.0064(2)	0.0078(2)	0	0.00213(15)	0
M(3)	0.0097(4)	0.0056(3)	0.0079(3)	0	0.0004(2)	0
M(4)	0.0129(2)	0.00996(19)	0.0129(2)	0	0.00672(14)	0
T(1)	0.00744(18)	0.00632(17)	0.00809(17)	−0.00056(11)	0.00141(13)	−0.00073(11)
T(2)	0.00715(18)	0.00686(17)	0.00760(16)	−0.00005(10)	0.00176(12)	−0.00082(11)
O(1)	0.0093(4)	0.0096(4)	0.0104(4)	−0.0004(3)	0.0020(3)	−0.0008(3)
O(2)	0.0082(4)	0.0105(4)	0.0107(4)	0.0003(3)	0.0020(3)	−0.0001(3)
O(3)	0.0106(6)	0.0136(6)	0.0119(6)	0	0.0023(5)	0
O(4)	0.0136(5)	0.0097(4)	0.0135(4)	−0.0004(3)	0.0039(3)	−0.0028(3)
O(5)	0.0112(4)	0.0169(5)	0.0129(4)	0.0051(3)	0.0014(3)	0.0002(3)
O(6)	0.0121(5)	0.0143(5)	0.0151(4)	−0.0042(3)	0.0040(4)	0.0001(3)
O(7)	0.0125(7)	0.0148(7)	0.0226(7)	0	0.0018(5)	0

that *M*(2) contains smaller and highly-charged ions. All Al was placed in the *M*(2) site. The *M*(1), *M*(2) and *M*(3) adjusted site populations can be derived from site-scattering refinement results,

TABLE 6. Selected interatomic distances in oxo-magnesio-hastingsite and oxykaersutite.

	Oxo-magnesio-hastingsite	Oxykaersutite*		Oxo-magnesio-hastingsite	Oxykaersutite*
M(1)–O(3)	2.0142(10) ×2	1.988(5)	*T*(2)–O(4)	1.6055(11)	1.615(4)
M(1)–O(1)	2.0477(10) ×2	2.037(5)	*T*(2)–O(2)	1.6362(11)	1.644(4)
M(1)–O(2)	2.1488(11) ×2	2.173(2)	*T*(2)–O(5)	1.6495(10)	1.651(5)
<*M*(1)–O>	2.070	2.066	*T*(2)–O(6)	1.6661(11)	1.663(4)
			<*T*(2)–O>	1.639	1.64
M(2)–O(4)	1.9897(11) ×2	1.981(5)			
M(2)–O(2)	2.0905(10) ×2	2.085(5)	*A*(m)–*A*(m)	0.540(15)	
M(2)–O(1)	2.1200(10) ×2	2.106(5)	*A*(m)–*A*(m′)	0.990(19)	
<*M*(2)–O>	2.067	2.057	*A*(m)–O(7)	2.456(5)	
			A(m)–O(7)	2.474(5)	
M(3)–O(3)	2.0657(14) ×2	2.0767(7)	*A*(m)–O(6)	2.899(5) ×2	
M(3)–O(1)	2.0762(10) ×4	2.084(4)	*A*(m)–O(5)	3.014(3) ×2	
<*M*(3)–O>	2.073	2.067			
			A(m')–*A*(m)	0.990(19)	
M(4)–O(4)	2.3485(10) ×2		*A*(m′)–*A*(m′)	1.44(2)	
M(4)–O(2)	2.4182(10) ×2		*A*(m′)–O(7)	2.543(6)	
M(4)–O(6)	2.5626(11) ×2		*A*(m′)–O(7)	2.564(7)	
M(4)–O(5)	2.6691(11) ×2		*A*(m′)–O(6)	2.622(7) ×2	
<*M*(4)–O>	2.4996		*A*(m′)–O(5)	3.010(3) ×2	
			A(m′)–O(7)	3.081(11)	
T(1)–O(1)	1.6603(11)	1.684(4)	*A*(m′)–O(3)	3.186(10)	
T(1)–O(7)	1.6609(7)	1.665(2)	*A*(m′)–O(5)	3.243(6) ×2	
T(1)–O(6)	1.6766(10)	1.682(5)			
T(1)–O(5)	1.6811(11)	1.689(4)			
<*T*(1)–O>	1.670	1.68			

* Hawthorne and Grundy (1973).

microprobe analyses and average bond lengths (Table 4). We omit the consideration of Mn as its scattering is within the standard deviations of the refined scattering values.

The $A(m)$ site was assigned to Na and the $A(m)'$ site to K. This assignment was done in agreement with the previous works of Tait *et al.* (2005) and Hawthorne *et al.* (1996). Occupancies of both sites were refined with their isotropic-displacement parameters and it was decided not to constrain them.

Oxo-magnesio-hastingsite has a large (but not >2.0 a.p.f.u.) Al content. Distribution of Al in the $T(1)$ tetrahedral site was calculated from the equation suggested first by Oberti *et al.* (1995) and further revised by Oberti *et al.* (2007). Obviously, Al tends to occupy the $T(1)$ site in preference to the $T(2)$ site, as confirmed by the $<T(1)-O>$ and $<T(2)-O>$ bond lengths (Table 6).

The parameters from single-crystal analysis used in calculations of X-ray powder diffraction data for the ferri-kaersutite were collected using a

TABLE 7. X-ray powder diffraction data for oxo-magnesio-hastingsite.

I_{meas}	d_{meas}	I_{calc}	d_{calc}	$h\ k\ l$	I_{meas}	d_{meas}	I_{calc}	d_{calc}	$h\ k\ l$
17	9.05	16	9.03	0 2 0	8	1.8520	4	1.8509	$\bar{1}$ 7 2
25	8.45	63	8.43	1 1 0	4	1.8068	4	1.8067	0 10 0
19	4.921	15	4.917	$\bar{1}$ 1 1	3	1.7611	6	1.7611	$\bar{5}$ 1 2
18	4.519	16	4.517	0 4 0	2	1.7565	<1	1.7555	$\bar{1}$ 1 3
4	3.988	8	3.987	1 1 1	26	1.6929	9	1.6927	$\bar{1}$ 3 3
14	3.897	8	3.896	$\bar{1}$ 3 1	9	1.6786	7	1.6783	0 2 3
62	3.383	69	3.382	1 3 1	13	1.6504	33	1.6499	4 6 1
30	3.281	45	3.279	2 4 0	6	1.6404	9	1.6397	4 8 0
25	3.132	74	3.131	3 1 0	13	1.6192	13	1.6193	1 11 0
6	2.951	5	2.950	$\bar{1}$ 5 1	39	1.5854	28	1.5850	$\bar{1}$ 5 3
20	2.939	39	2.938	2 2 1	3	1.5542	9	1.5534	4 0 2
7	2.813	14	2.812	3 3 0	6	1.5460	17	1.5454	$\bar{6}$ 0 2
20	2.751	38	2.750	$\bar{3}$ 3 1	48	1.5211	33	1.5208	$\bar{2}$ 6 3
97	2.708	100	2.707	1 5 1	3	1.5110	3	1.5109	$\bar{4}$ 8 2
75	2.596	61	2.596	0 6 1	13	1.5061	15	1.5056	0 12 0
8	2.562	5	2.562	0 0 2	3	1.5024	8	1.5019	5 5 1
100	2.555	75	2.555	$\bar{2}$ 0 2	4	1.4756	4	1.4751	$\bar{2}$ 10 2
2	2.459	1	2.458	$\bar{2}$ 2 2	4	1.4691	3	1.4689	4 4 2
2	2.419	1	2.420	$\bar{2}$ 6 1	5	1.4599	7	1.4594	3 11 0
5	2.387	8	2.387	3 5 0	4	1.4566	4	1.4562	$\bar{1}$ 7 3
29	2.349	42	2.349	$\bar{3}$ 5 1	16	1.4448	43	1.4445	$\bar{6}$ 6 1
7	2.338	18	2.337	$\bar{4}$ 2 1	2	1.4385	3	1.4381	$\bar{5}$ 3 3
20	2.304	17	2.304	$\bar{1}$ 7 1	4	1.3708	7	1.3704	$\bar{5}$ 5 3
17	2.296	18	2.296	$\bar{3}$ 1 2	8	1.3420	11	1.3416	1 11 2
3	2.228	2	2.228	0 4 2	4	1.3401	5	1.3402	$\bar{3}$ 11 2
16	2.224	9	2.224	$\bar{2}$ 4 2	6	1.3345	8	1.3343	2 6 3
6	2.182	4	2.182	1 7 1	4	1.3161	2	1.3158	1 13 1
36	2.162	40	2.162	2 6 1	11	1.3129	9	1.3127	$\bar{1}$ 1 4
6	2.140	4	2.140	$\bar{1}$ 5 2	2	1.2992	2	1.2987	$\bar{3}$ 9 3
13	2.044	22	2.044	2 0 2	15	1.2978	18	1.2980	$\bar{2}$ 12 2
10	2.033	18	2.033	$\bar{4}$ 0 2	3	1.2863	3	1.2858	$\bar{1}$ 3 4
11	2.017	18	2.016	3 5 1	2	1.2844	2	1.2845	$\bar{3}$ 3 4
4	2.004	5	2.004	3 7 0	5	1.2816	3	1.2817	6 6 1
8	1.9649	8	1.9644	1 9 0	6	1.2777	7	1.2774	$\bar{4}$ 0 4
5	1.9497	4	1.9492	$\bar{3}$ 5 2	2	1.2324	<1	1.2324	0 4 4
12	1.8692	12	1.8694	$\bar{1}$ 9 1	2	1.2305	3	1.2307	$\bar{2}$ 14 1
2	1.8626	3	1.8620	2 4 2	6	1.2043	12	1.2042	$\bar{5}$ 11 2

The discrepancies between observed and calculated intensities are caused by preferred (110) orientation of the grains in the powder.

STOE STADI P diffractometer (St Petersburg State University) and are given in Table 7 (in Å for CuKα_1, λ = 1.540598 Å). Unit-cell parameters refined from the powder data are as follows a = 9.884(2), b = 18.069(2), c = 5.310(1) Å, β = 105.30(1)°.

Stable H and O isotopic composition

The H and O isotope compositions were determined at the Institute for Geological and Geochemical Research, Budapest and at the University of Lausanne, Switzerland. The O isotope compositions of silicate minerals were measured using a CO_2 laser (Rumble and Hoering, 1994; Kasemann *et al.*, 2001). The following $\delta^{18}O$ values were obtained for international reference materials in the course of this study: NBS-28 quartz 9.60±0.07‰ (2σ, N = 12; recommended value: 9.64‰), NBS-30 biotite 4.95±0.01‰ (2σ, N = 2; recommended value: 5.1‰), UWG-2 garnet 5.83±0.03‰ (2σ, N = 3; recommended value: 5.8‰, Valley *et al.*, 1995). Based on these data and the reproducibility of duplicate measurements, the $\delta^{18}O$ values of our samples are precise to within 0.15‰. The H_2O contents and H isotope compositions were determined using two methods: (i) samples OL 22, OL 313 and OL 246 – vacuum heating in silica tubes and subsequent reaction of liberated H_2O with Zn alloy (Indiana University, Bloomington) followed by D/H ratio analyses using a Finnigan MAT delta S dual inlet mass spectrometer at the Institute for Geological and Geochemical Research, Budapest (Vennemann and O'Neil, 1993; Demény *et al.*, 1997); and (ii) samples DT -/11, LL 1/5, LL -/4 and LL 3/4 – H_2 liberation using a high-temperature conversion elemental analyser (TC/EA) coupled to a Finnigan MAT delta plus XL mass spectrometer at the University of Lausanne (Sharp *et al.*, 2001). The raw data for H isotope compositions were normalized using NBS-30 biotite and two in-house standards (Kaol#17 kaolinite and G1 biotite). The H isotope compositions of the laboratory standards measured in this study are reproducable to within ±2‰. A δD value of −65.0‰ was obtained for the NBS-30 biotite standard (recommended value is −65.7‰) analysed along with the five samples measured by dual inlet technique. The precision of H_2O content is better than 0.1 wt.%, on the basis of repeated measurements of NBS-30 and in-house standards. The results are expressed in the δ-notation ($\delta = (R_1/R_2 - 1)\cdot 1000$ where R_1 and R_2 are the D/H or $^{18}O/^{16}O$ ratios in the sample and the standard, respectively) in permil (‰) relative to V-SMOW (Table 8).

The δD values in the oxo-magnesio-hastingsite and magnesio-hastingsite range from −50.5 to −32.7‰, and the $\delta^{18}O$ values in the minerals vary between 5.27 and 5.85‰ (Table 8). The hydrogen and oxygen isotopic compositions show positive correlations between determined values (R = 0.82) (Fig. 6*a*), and neither is correlated with H_2O content.

The oxygen isotopic composition of the amphiboles studied is within the accepted range for pristine mantle-derived rocks, which is considered to lie between 5 and 6‰ (Kyser, 1986; Mattey *et al.*, 1994; Chazot *et al.*, 1997; Hoefs, 2009). Amphibole megacrysts occurring in kimberlites, olivine melilitites, olivine nephelinites, basanites and alkaline basalts from other occurrences show $\delta^{18}O$ values between 4.6 and 6.0 (e.g. Boettcher and O'Neil, 1980; Dawson and Smith, 1982; Hergner and Vennemann, 1997). In contrast, the hydrogen-isotope composition in the

TABLE 8. O and H isotope data (in ‰, V-SMOW) for oxo-magnesio-hastingsite and magnesio-hastingsite.

Sample	Location	$\delta^{18}O$	δD
OL 22	Deeti	5.58	−41.7
DT -/11	Deeti	5.35	−45.4
OL 313	Loolmurwak	5.85	−32.7
LL 1/5	Loluni	5.62	−48.1
LL -/4	Loluni	5.67	−45.5
LL 3/4	Loluni	5.57	−43.2
OL 246	Oldoinyo Lengai – Dorobo	5.80	−38.2
OL 165	Oldoinyo Lengai – Lalarasi	5.27	−50.5

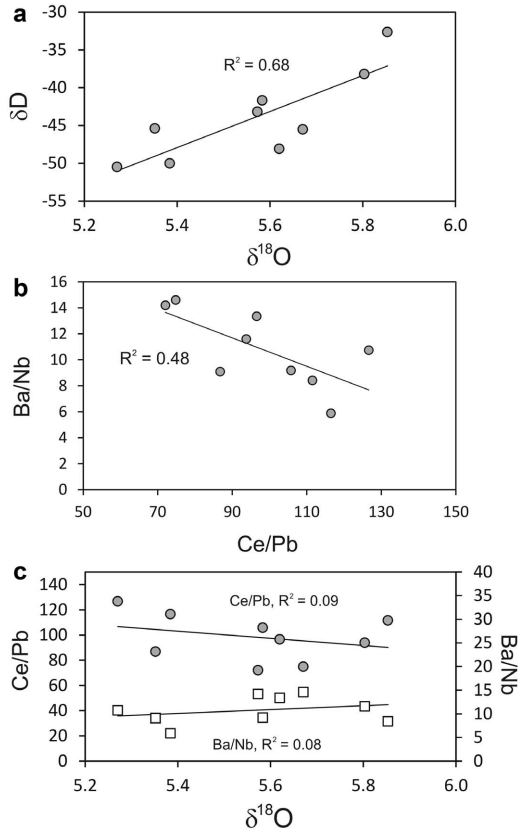

FIG. 6. Stable hydrogen and oxygen isotope compositions (in ‰ relative to V-SMOW) and Ba/Nb and Ce/Pb ratios in the oxo-magnesio-hastingsite and magnesio-hastingsite.

oxo-magnesio-hastingsite and magnesio-hastingsite studied shows values which are higher than the assumed mantle range (−60 to −80‰: Boettcher and O'Neil, 1980; Bell and Ihinger, 2000), but overlap with the range assumed for subducted slab components (~ −40‰, Magaritz and Taylor, 1976; Agrinier *et al.*, 1993; Demény *et al.*, 2005; Shaw *et al.*, 2008). Available data for δD values in amphibole group minerals such as pargasite or kaersutite occurring as megacrysts in mantle-derived rocks indicate a very large range in their hydrogen composition – between −20 and −120‰ (Bell and Ihinger, 2000, and references therein).

Origin of the amphiboles

The oxo-magnesio-hastingsite, magnesio-hastingsite and possibly kaersutite megacrysts from the Deeti, Loluni, Loolmurwak cones and craters are clearly of magmatic origin from a silica-undersaturated alkaline melt. Given the fact that huge grains of the amphiboles occur, it is certainly a liquidus phase. Inclusions of diopside, particularly in the oxo-magnesio-hastingsite from Deeti, indicate that the liquidus assemblage changed from clinopyroxene to amphibole during fractionation of the magma, probably in a deep-seated chamber, in accordance with the typical H_2O enrichment and more oxidizing conditions during fractionation that broadly basaltic magmas show in the absence of a solid phase oxygen buffer assemblage. The growth of oxo-magnesio-hastingsite around or at the expense of earlier formed diopside could principally also be explained by addition of a water-bearing, oxidizing fluid to the evolving crystal-melt mush, but the size of the crystals argues for a deep-seated origin for them. The fact that amphiboles occur as rounded crystals, while clinopyroxene (diopside) forms distinct crystal surfaces is remarkable, particularly as the amphibole grows around clinopyroxene. Either this is a kinetic effect (pyroxene is less resorbed than amphibole during late melt evolution), or small variations in component (especially silica) activity may destabilize amphibole leading to resorption, while pyroxene remains stable. Given the low water content of the oxo-magnesio-hastingsite, variations in H_2O activity are probably of minor importance.

On the basis of mineralogical and geochemical studies of the Deeti cone tuffs Johnson *et al.* (1997) suggested that the observed suite of host melilitite, xenoliths and megacrysts might be an indication of a depth of ~60–90 km for the magma source. The assemblage of amphibole, diopside and phlogopite megacrysts at Deeti and other cones and craters is considered to be a high-pressure equivalent of olivine melilitite (Tilley and Yoder, 1968; Dawson, 2008).

Observed variations in the oxygen and hydrogen isotopic compositions of the studied amphiboles, as well as contents of trace elements provide additional information about the origin of the minerals.

It is well known that H and O isotope compositions in amphiboles can depend on a number of different processes (e.g. Demény *et al.*, 2006). Following crystallization from the magma, amphiboles are prone to degassing due to pressure decrease, isotope exchange with magmatic or external H_2O at decreasing temperatures, or

weathering with the formation of secondary H-bearing minerals. The latter process can be detected on the basis of elevated H_2O contents. As the $\delta^{18}O$ values in the oxo-magnesio-hastingsite and magnesio-hastingsite show no change with H_2O contents, we conclude that weathering did not play a role in the observed stable isotope variations.

Isotope exchange with magmatic fluids at decreasing temperatures may explain the increased $\delta^{18}O$ values (Zheng, 1993). However, in that case the δD values should show a decrease (Suzuoki and Epstein, 1976) or remain constant (Graham *et al.*, 1984) with decreasing temperatures and, thus, increasing $\delta^{18}O$ values, opposite to what is observed in the samples studied (Fig. 6*a*).

Hydrogen loss from the amphibole structure during degassing can explain the elevation of δD values (Demény *et al.*, 2006), but it is unlikely to be a cause of the coupled $\delta D - \delta^{18}O$ shift. Additionally, the δD values show no correlation with the H_2O contents that would be expected if amphibole degassing was the determining process. The Fe^{3+} contents would also argue against significant amphibole degassing, as the oxo-magnesio-hastingsite with extreme Fe^{3+} enrichment has δD and $\delta^{18}O$ values just in the average range of the other samples.

These considerations lead to the conclusion that the stable isotope compositions of the oxo-magnesio-hastingsite and magnesio-hastingsite were determined by variations in their host magmas' compositions. δD and $\delta^{18}O$ elevations can usually be attributed to a contribution of crustal component that is typically enriched in D and ^{18}O relative to the upper mantle. This crustal contamination could be detected by trace element ratios such as Ce/Pb and Ba/Nb. These ratios show a negative correlation ($R = -0.69$) in the amphiboles (Fig. 6*b*), so involvement of a crustal component can be assumed. The $\delta^{18}O$ values display negative and positive relationships with Ce/Pb and Ba/Nb, respectively, which are the expected directions; however, the correlations are very weak and not significant (Fig. 6*c*). The δD values show no correlations with these trace element ratios, so the δD variation is not related to simple addition of crustal material to the mantle-derived melt.

The resolution of these discrepancies lies in the assumption of different processes that induce changes in δD and $\delta^{18}O$ values independently. The oxo-magnesio-hastingsite with its extreme Fe^{3+} enrichment and low H_2O content has a

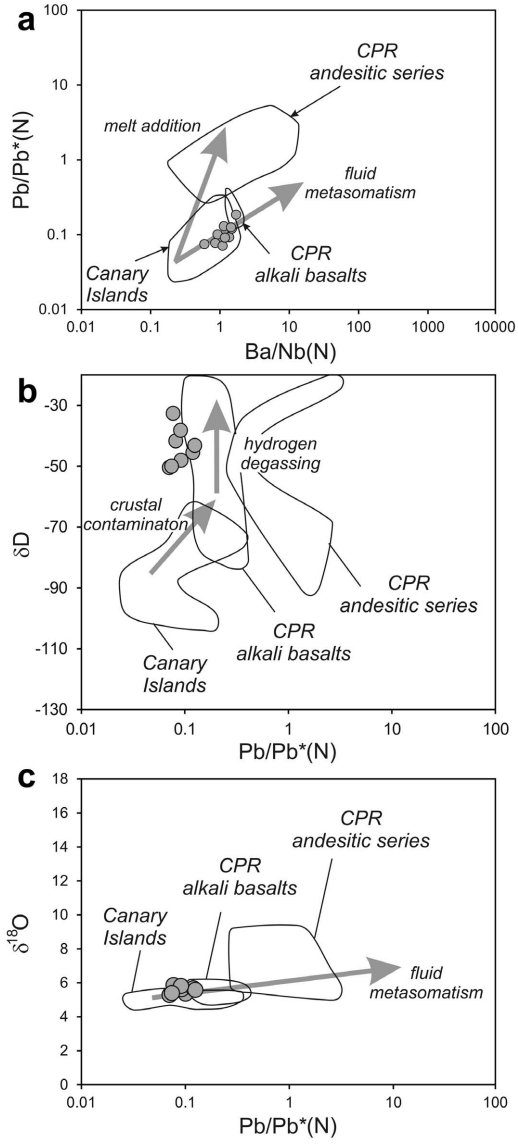

FIG. 7. (*a*) Pb/Pb*(N) ratios *vs*. Ba/Nb(N) ratios (normalized to primitive mantle, Hofmann, 1988) of the oxo-magnesio-hastingsite and magnesio-hastingsite. Fields for amphiboles from the Canary Islands and from the Carpathian-Pannonian Region (CPR) are from Demény *et al.* (2012). See text for explanations of arrows; (*b*) Pb/Pb*(N) ratios normalized to primitive mantle *vs*. hydrogen and (*c*) oxygen isotope compositions (in ‰ relative to V-SMOW) of the oxo-magnesio-hastingsite and magnesio-hastingsite.

crucial role in the interpretation of the δD data. As it has a δD value that falls in the range of the samples studied, it suggests that the Fe^{3+} enrichment and H_2O depletion were reached by the host melt probably due to H_2 degassing. Depending on the starting H_2O content and δD value, as well as on the H_2 degassing degree, different magma batches may reach different D-enrichment levels. These different magma batches have their own evolution pathways, including partial melting, fractional crystallization and crustal contamination, leading to $\delta^{18}O$ and trace element variations. The most primitive melt could be represented by the amphibole with the lowest δD and $\delta^{18}O$ values. As discussed above, the $\delta^{18}O$ value of 5.2‰ corresponds to the normal mantle-derived amphibole compositions, whereas the δD value of −50‰ is significantly greater than usual mantle compositions (e.g. Boettcher and O'Neil, 1980; Kyser and O'Neil, 1984; Kyser, 1986; Agrinier *et al.*, 1993), fitting crustal slab compositions. This situation can be produced by metasomatism of crustal fluids, in which case hydrogen is dominated by the fluid; whereas oxygen is buffered by the silicate melt. In a comprehensive study on mantle-derived amphiboles, Demény *et al.* (2012) compared trace element ratios and stable isotope compositions to detect mantle contamination processes and to make a distinction between the effects of melt addition and fluid metasomatism. Combination of certain trace-element ratios (Ba/Nb and $Pb/\sqrt{[Ce \cdot Pr]}$, called Pb/Pb* – Marks *et al.* (2004)) with stable H and O isotope data was found to be effective in this distinction. The amphiboles studied in this paper have Ba/Nb(N) and Pb/Pb*(N) values (normalized to the primitive mantle (Hofmann, 1988)) of 1.10±0.30 and 0.09±0.02, respectively, which are transitional between those for amphiboles related to plume-derived melts and for basalts and andesites formed in the subduction-related environment of the Carpathian–Pannonian Region (Fig. 7*a*). The vertical array of hydrogen isotope compositions in the δD−Pb/Pb*(N) plot (Fig. 7*b*) indicate dehydrogenation (H_2 degassing, see Demény *et al.*, 2006) with starting compositions higher than the values for uncontaminated mantle. This indicates that the host melt of the amphibole megacrysts was contaminated by crustal material and experienced hydrogen degassing. The $\delta^{18}O$ and Pb/Pb*(N) data plot on the fluid metasomatic array (Fig. 7*c*) defined by Demény *et al.* (2012), suggesting that the addition of a crustal component was induced by fluid infiltration from a subducted slab. It is important to note that the influence of a subducted(?) old Archaean upper continental crust component on the lithospheric mantle composition beneath northern Tanzania has been suggested on the basis of isotopic studies of mantle xenoliths from Lashaine, which is close to the area studied (Aulbach *et al.*, 2011). On a Zr−Nb amphibole plot of Coltorti *et al.* (2007) data from the samples studied fall in a transitional field between intraplate and suprasubduction amphiboles (Fig. 8), with the one exception of an Oldoinyo Lengai-Lalarasi sample.

Conclusions

The amphibole megacrysts occurring in explosive rocks in the Lake Natron–Engaruka volcanic field are represented by oxo-magnesio-hastingsite,

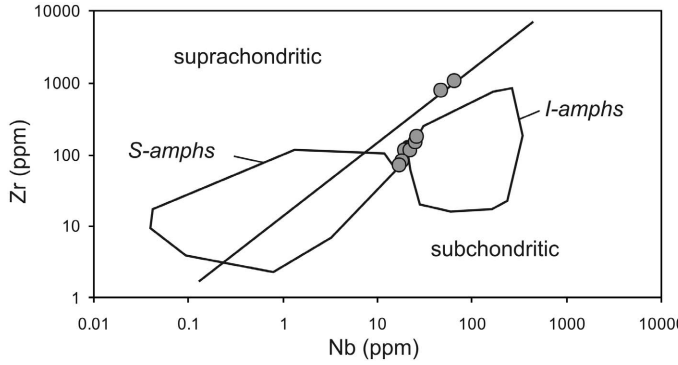

FIG. 8. Zr *vs*. Nb discrimination diagram after Coltorti *et al.* (2007). I-amph: intraplate amphiboles, S-amph: suprasubduction amphiboles.

magnesio-hastingsite and possibly kaersutite. The new mineral oxo-magnesio-hastingsite is a Ti-rich amphibole, it contains a significant amount of the $NaCa_2(Mg_3Fe^{3+}Ti)(Al_2Si_6)O_{22}O_2$ endmember and amphiboles with similar compositions are known from several other localities (e.g. Dawson and Smith, 1982; Dyar *et al.*, 1993; Nasir and Al-Rawas, 2006).

The combined evaluation of H_2O and Fe^{3+} contents, H and O isotope compositions and trace element concentrations lead to the conclusion that late-stage processes such as amphibole degassing, isotope exchange at decreasing temperatures and weathering did not affect the compositions of the minerals. The observed compositional variations most likely reflect those of the host magma batches that have experienced different degrees of magmatic evolution (partial melting, fractional crystallization, H_2 degassing and crustal contamination). The observed iron enrichment and low water content of the oxo-magnesio-hastingsite from the Deeti cone can be related to strong H_2 degassing from the host magma from which the amphibole crystallized. The initial magmatic stable H and O isotope compositions are ~−50 and 5.2‰ that indicates a mantle source metasomatized by slab-derived fluids. The metasomatic effect is also supported by trace element ratios generally used for the detection of crustal components (Ba/Nb, Ce/Pb and Pb/$\sqrt{}$[Ce·Pr]).

Acknowledgements

We are grateful to Polina Zaitseva for help with sample photography, Nikita Chukanov for help with water analysis in sample OL 22 AZ, and Barry Dawson for comments and a field photo. We also thank reviewers John Schumacher for his comments and, particularly, Roberta Oberti for valuable discussion about amphibole crystal chemistry. At various stages this work was supported by Deutsche Forschungsgemeinschaft (Germany), Alexander von Humboldt Stiftung (Germany), Marie Curie IIF (6^{th} European Community Framework Programme), St Petersburg State University, including Geomodel and Diffraction Centre (Russia), the Natural History Museum (UK) and University of Lausanne (Switzerland).

References

Agrinier, P., Mével, C., Bosch, D. and Javoy, M. (1993) Metasomatic hydrous fluids in amphibole peridotites from Zabargad Island (Red Sea). *Earth and Planetary Science Letters*, **120**, 187−205.

Apopei, A.I., Buzgar, N. and Buzatu, A. (2011) Raman and infrared spectroscopy of kaersutite and certain common amphiboles. *Analele Universităţii "Al. I. Cuza" din Iaşi - Seria Geologie (AUI-G)*, **57**(2), 35−58.

Aulbach, S., Rudnick, R.L. and McDonough, W.F. (2011) Evolution of the lithospheric mantle beneath the East African Rift in Tanzania and its potential signatures in rift magmas. *Geological Society of America Special Papers*, **478**, 105−125.

Bell, D.R. and Ihinger, P.D. (2000) The isotopic composition of hydrogen in nominally anhydrous mantle minerals. *Geochimica et Cosmochimica Acta*, 64, 2109−2118.

Bell, K. and Keller, J. (Eds) (1995) *Carbonatite Volcanism - Oldoinyo Lengai and the Petrogenesis of Natrocarbonatites*. IAVCEI Proceedings in Volcanology **4**, Springer, Berlin Heidelberg.

Boettcher, A.L. and O'Neil, J.R. (1980) Stable isotope, chemical, and petrographic studies of high-pressure amphiboles and micas: evidence for metasomatism in the mantle source regions of alkali basalts and kimberlites. *American Journal of Science*, **280-A**, 594−621.

Chazot, G., Lowry, D., Menzies, M. and Mattey, D. (1997) Oxygen isotopic composition of hydrous and anhydrous mantle peridotites. *Geochimica et Cosmochimica Acta*, **61**, 161−169.

Church, A.A. (1996) *The petrology of the Kerimasi carbonatite volcano and the carbonatites of Oldoinyo Lengai with a review of other occurrences of extrusive carbonatites*. PhD thesis, University of London

Coltorti, M., Bonadiman, C., Faccini, B., Grégoire, M., O'Reilly, S.Y. and Powell, W. (2007) Amphiboles from suprasubduction and intraplate lithospheric mantle. *Lithos*, **99**, 68−84.

Dawson, J.B. (1962) The geology of Oldoinyo Lengai. *Bulletin Volcanologique*, **24**, 348−387.

Dawson, J.B. (1964) Carbonatitic volcanic ashes in Northern Tanganyika. *Bulletin Volcanologique*, **27**, 81−91.

Dawson, J.B. (2008) *The Gregory Rift Valley and Neogene-Recent Volcanoes of Northern Tanzania*. Memoir of the Geological Society of London, **33**.

Dawson, J.B. and Powell, D.G. (1969) The Natron-Engaruka explosion crater area, Northern Tanzania. *Bulletin Volcanologique*, **33**, 791−817.

Dawson, J.B. and Smith, J.V. (1982) Upper-mantle amphiboles: a review. *Mineralogical Magazine*, **45**, 35−46.

Dawson, J.B. and Smith, J.V. (1988) Metasomatised and veined upper-mantle xenoliths from Pello Hill, Tanzania: evidence for anomalously-light mantle

beneath the East African Rift Valley. *Contributions to Mineralogy and Petrology*, **100**, 510–527.

Dawson, J.B., Smith, J.V. and Jones, A.P. (1985) A comparative study of bulk rock and mineral chemistry of olivine melilitites and associated rocks from East and South Africa. *Neues Jahrbuch für Mineralogie - Abhandlungen*, **152**, 143–175.

Della Ventura, G., Oberti, R., Hawthorne, F.C. and Bellatreccia, F. (2007) FTIR spectroscopy of Ti-rich pargasites from Lherz and the detection of O^{2-} at the anionic O3 site in amphiboles. *American Mineralogist*, **92**, 1645–1651.

Demény, A., Sharp, Z.D. and Pfeifer, H-R. (1997) Mg-metasomatism and formation conditions of Mg-chlorite-muscovite-quartzphyllites (leucophyllites) of the Eastern Alps (W. Hungary) and their relations to Alpine whiteschists. *Contributions to Mineralogy and Petrology*, **128**, 247–260.

Demény, A., Vennemann, T.W., Homonnay, Z., Milton, A., Embey-Isztin, A. and Nagy, G. (2005) Origin of amphibole megacrysts in the Plio-Pleistocene basalts of the Carpathian–Pannonian Region. *Geologica Carpathica*, **56**, 179–189.

Demény, A., Vennemann, T.W., Harangi, Sz., Homonnay, Z. and Fórizs, I. (2006) H_2O–δD–Fe^{III} relations of dehydrogenation and dehydration processes in magmatic amphiboles. *Rapid Communications in Mass Spectrometry*, **20**, 919–925.

Demény, A., Harangi, S., Vennemann, T.W., Casillas, R., Horváth, P., Milton, A.J., Mason, P.R.D. and Ulianov, A. (2012) Amphiboles as indicators of mantle source contamination: combined evaluation of stable H and O isotope compositions and trace element ratios. *Lithos*, **152**, 141–156.

Dyar, M.D., Mackwell, S.J., McGuire, A.V., Cross, L.R. and Robertson, J.D. (1993) Crystal chemistry of Fe^{3+} and H^+ in mantle kaersutite: implications for mantle metasomatism. *American Mineralogist*, **78**, 968–979.

Graham, C.M., Harmon, R.S. and Sheppard, S.M.F. (1984) Experimental hydrogen isotope studies: hydrogen exchange between amphibole and water. *American Mineralogist*, **69**, 128–138.

Hawthorne, F.C. and Grundy, H.D. (1973) The crystal chemistry of the amphiboles II. Refinement of the crystal structure of oxy-kaersutite. *Mineralogical Magazine*, **39**, 390–400.

Hawthorne, F.C., Oberti, R., Cannillo, E., Sardone, N., Zanetti, A., Grice, J.D. and Ashley, P.M. (1995)A new anhydrous amphibole from the Hoskins mine, Grenfell, New South Wales, Australia: description and crystal structure of ungaretiite, $NaNa_2(Mn^{2+}_2Mn^{3+}_3)Si_8O_{22}O_2$. *American Mineralogist*, **80**, 165–172.

Hawthorne, F.C., Ungaretti, L. and Sardonne, N. (1996) Sodium at the A site in clinoamphiboles: the effects of composition on patterns of order. *The Canadian Mineralogist*, **34**, 577–593.

Hawthorne, F.C., Cooper, M.A., Grice, J.D. and Ottolini, L. (2000) A new anhydrous amphibole from the Eifel region, Germany: description and crystal structure of obertiite, $NaNa_2(Mg_3Fe^{3+}Ti^{4+})Si_8O_{22}O_2$. *American Mineralogist*, **85**, 236–241.

Hawthorne, F.C., Oberti, R., Harlow, G.E., Maresch, W.V., Martin, R.F., Schumacher, J. and Welch, M.D. (2012) Nomenclature of the amphibole supergroup. *American Mineralogist*, **97**, 2031–2048.

Hay, R.L. (1983) Natrocarbonatite tephra of Kerimasi volcano, Tanzania. *Geology*, **11**, 599–602.

Hergner, E. and Vennemann, T.W. (1997) Role of fluids in the origin of Tertiary European intraplate volcanism: evidence from O, H, and Sr isotopes in melilitites. *Geology*, **25**, 1035–1038.

Hoefs, J. (2009) *Stable Isotope Geochemistry*. Sixth Edition. Springer, Berlin, Heidelberg.

Hofmann, A.W. (1988) Chemical differentiation of the Earth: the relationship between mantle, continental crust, and oceanic crust. *Earth and Planetary Science Letters*, **90**, 297–314.

Johnson, L.H., Jones, A.P., Church, A.A. and Taylor, W.R. (1997) Ultramafic xenoliths and megacrysts from a melilitite tuff cone, Deeti, northern Tanzania. *Journal of African Earth Sciences*, **25**, 29–42.

Kasemann, S., Meixner, A., Rocholl, A., Vennemann, T., Schmitt, A. and Wiedenbeck, M. (2001) Boron and oxygen isotope composition of certified reference materials NIST SRM 610/612, and reference materials JB-2G and JR-2G. *Geostandards Newsletter*, **25**, 405–416.

Keller, J. and Krafft, M. (1990) Effusive natrocarbonatite activity of Oldoinyo Lengai, June 1988. *Bulletin of Volcanology*, **52**, 629–645.

Keller, J. and Zaitsev, A.N. (2012) Geochemistry and petrogenetic significance of natrocarbonatites at Oldoinyo Lengai, Tanzania: composition of lavas from 1988 to 2007. *Lithos*, **148**, 45–53.

Keller, J., Zaitsev, A.N. and Wiedenmann, D. (2006) Primary magmas at Oldoinyo Lengai: the role of olivine melilitites. *Lithos*, **91**, 150–172.

Keller, J., Klaudius, J., Kervyn, M., Ernst, G.G.J. and Mattsson, H.B. (2010) Fundamental changes in the activity of the natrocarbonatite volcano Oldoinyo Lengai, Tanzania. I. New magma composition during the 2007–2008 explosive eruptions. *Bulletin of Volcanology*, **72**, 893–912.

Kyser, T.K. (1986) Stable isotope variations in the mantle. *Reviews in Mineralogy and Geochemistry*, 16, 141–164.

Kyser, T.K. and O'Neil, J.R. (1984) Hydrogen isotope systematics of submarine basalts. *Geochimica et Cosmochimica Acta*, **48**, 2123–2133.

Magaritz, M. and Taylor, H.P., Jr. (1976) Oxygen, hydrogen and carbon is otope studies of the Franciscan formation, Coast Ranges, California. *Geochimica et Cosmochimica Acta*, **40**, 215–234.

Mariano, A.N. and Roeder, P.L. (1983) Kerimasi: a neglected carbonatite volcano. *The Journal of Geology*, **91**, 449–455.

Marks, M., Halama, R., Wenzel, T. and Markl, G. (2004) Trace element variations in clinopyroxene and amphibole from alkaline to peralkaline syenites and granites: implications for mineral–melt trace-element partitioning. *Chemical Geology*, **211**, 185–215.

Mattey, D., Lowry, D. and Macpherson, C. (1994) Oxygen isotope composition of mantle peridotite. *Earth and Planetary Science Letters*, **128**, 231–241.

Mattsson, H.B. and Tripoli, B.A. (2011) Depositional characteristics and volcanic landforms in the Lake Natron–Engaruka monogenetic field, northern Tanzania. *Journal of Volcanology and Geothermal Research*, **203**, 23–34.

Nasir, S. and Al-Rawas, A.D. (2006) Mössbauer characterization of upper mantle ferrikaersutite. *American Mineralogist*, **91**, 1163–1169.

Oberti, R., Ungaretti, L., Cannillo, E., Hawthorne, F.C. and Memmi, I. (1995) Temperature-dependent Al order-disorder in the tetrahedral double-chain of *C*2/*m* amphiboles. *European Journal of Mineralogy*, **7**, 1049–1063.

Oberti, R., Hawthorne, F.C., Cannilo, E. and Cámara, F. (2007) Long-range order in amphiboles. Pp. 125–172 in: *Amphiboles: Crystal Chemistry, Occurrence, and Health Issues* (F.C. Hawthorne, R. Oberti, G. Della Ventura and A. Mottana, editors). Reviews in Mineralogy and Geochemistry, **67**. Mineralogical Society of America and The Geochemical Society, Washington, D.C.

Reguir, E.P., Chakhmouradian, A.R., Nalden, N.M., Yang, P. and Zaitsev, A.N. (2008) Early magmatic and reaction-induced trends in magnetite from the carbonatites of Kerimasi, Tanzania. *The Canadian Mineralogist*, **46**, 879–900.

Rumble, D. and Hoering, T.C. (1994) Analysis of oxygen and sulfur isotope ratios in oxide and sulfide minerals by spot heating with a carbon dioxide laser in a fluorine atmosphrere. *Accounts of Chemical Research*, **27**, 237–241.

Sharp, Z.D., Atudorei, V. and Durakiewicz, T. (2001) A rapid method for determination of hydrogen and oxygen isotope ratios from water and hydrous minerals. *Chemical Geology*, **178**, 197–210.

Shaw, A.M., Hauri, E.H., Fischer, T.P., Hilton, D.R. and Kelley, K.A. (2008) Hydrogen isotopes in Mariana arc melt inclusions: implications for subduction dehydration and the deep Earth water cycle. *Earth and Planetary Science Letters*, **275**, 138–145.

Suzuoki, T. and Epstein, S. (1976) Hydrogen isotope fractionation between OH-bearing minerals and water. *Geochimica et Cosmochimica Acta*, **40**, 1229–1240.

Tait, K.T., Hawthorne, F.C., Grice, J.D., Ottolini, L. and Nayak, V.K. (2005) Dellaventuraite, $NaNa_2(MgMn_2TiLi)Si_8O_{22}O_2$, a new anhydrous amphibole from the Kajlidongri Manganese Mine, Jhabua District, Madhya Pradesh, India. *American Mineralogist*, **90**, 304–309.

Tiepolo, M., Zannetti, A. and Oberti, R. (1999) Detection, crystal-chemical mechanisms and petrological implications of $^{[6]}Ti^{4+}$ partitioning in pargasite and kaersutite. *European Journal of Mineralogy*, **11**, 345–354.

Tilley, C.E. and and Yoder, H.S., Jr. (1968) The pyroxenite facies conversion of volcanic and subvolcanic, melilite-bearing and other alkali ultramafic assemblages. *Carnegie Institution of Washington, Annual Report of the Director of the Geophysical Laboratory*, 1966–67, 457–460.

Valley, J.W., Kitchen, N., Kohn, M.J., Niendorf, C.R. and Spicizza, M.J. (1995) UWG-2, a garnet standard for oxygen isotope ratios: Strategies for high precision and accuracy with laser heating. *Geochimca et Cosmochimica Acta*, **59**, 5523–5531.

Vennemann, T.W. and O'Neil, J.R. (1993) A simple and inexpensive method of hydrogen isotope and water analyses of minerals and rocks based on zinc reagent. *Chemical Geology*, **103**, 227–234.

Wakefield, T.K.J., Jr. (1870) Routes of native caravans from the coast to the interior of Eastern Africa, chiefly from information given by Sádi Bin Ahédi, a native of a district near Gázi, in Udigo, a little north of Zanzibar. *Journal of the Royal Geographical Society of London*, **40**, 303–339.

Wiedenmann, D., Keller, J. and Zaitsev, A.N. (2010) Melilite-group minerals at Oldoinyo Lengai, Tanzania. *Lithos*, **118**, 112–118.

Williams, P.A., Hatert, F., Pasero, M. and Mills, S. J. (2011) New minerals and nomenclature modifications approved in 2011. *Mineralogical Magazine*, **75**, 2549–2561.

Zaitsev, A.N. (2010) Nyerereite from calcite carbonatite of Kerimasi volcano, northern Tanzania. *Geology of Ore Deposits*, **52**(7), 630–640.

Zaitsev, A.N., Williams, C.T., Britvin, S.N., Kuznetsova, I.V., Spratt, J., Petrov, S.V. and Keller, J. (2010) Kerimasite, $Ca_3Zr_2(Fe_2^{3+}Si)O_{12}$, a new garnet from carbonatites of Kerimasi volcano and surrounding explosion craters, northern Tanzania. *Mineralogical Magazine*, **74**, 841–858.

Zaitsev, A.N., Chakhmouradian, A.R., Siidra, O.I., Spratt, J., Williams, C.T., Stanley, C.J., Petrov, S.V., Britvin, S.N. and Polyakova, E.A. (2011) Fluorine-, yttrium- and lanthanide-rich cerianite-(Ce) from carbonatitic rocks of the Kerimasi volcano

and surrounding explosion craters, Gregory Rift, northern Tanzania. *Mineralogical Magazine*, **75**, 2813–2822.

Zheng, Y.F. (1993) Calculation of oxygen isotope fractionation in hydroxil-bearing silicates. *Earth and Planetary Science Letters*, **120**, 247–263.